Journal of Power Sources 273 (2015) 923–930

Contents lists available at ScienceDirect

Journal of Power Sources

journal homepage: www.elsevier.com/locate/jpowsour

Micro-size spherical TiO_2(B) secondary particles as anode materials for high-power and long-life lithium-ion batteries

Norio Takami, Yasuhiro Harada*, Takuya Iwasaki, Keigo Hoshina, Yorikazu Yoshida

Corporate Research & Development Center, Toshiba Corporation, 1, Komukai-Toshiba-cho, Saiwai-ku, Kawasaki 212-8582, Japan

HIGHLIGHTS

- Spherical TiO_2(B) secondary particles are used as anode for lithium-ion batteries.
- The spherical TiO_2(B) particles are advantageous for high electrode density.
- The spherical TiO_2(B) electrodes have superior electronic connective property.
- Spherical TiO_2(B) electrodes lead to high-rate capability and long-cycle life.
- The TiO_2(B)/NCM cell exhibits high-power and a long-life of more than 3000 cycles.

GRAPHICAL ABSTRACT

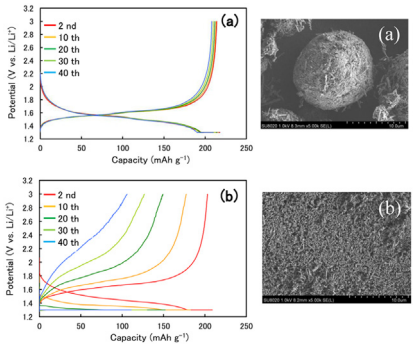

ARTICLE INFO

Article history:
Received 21 August 2014
Received in revised form
25 September 2014
Accepted 27 September 2014
Available online 5 October 2014

Keywords:
Spherical TiO_2(B) secondary particles
Anode materials
Lithium-ion batteries
High-rate capability
Long-cycle life

ABSTRACT

Electrochemical properties of micro-size spherical TiO_2(B) secondary particles have been investigated in order to develop TiO_2(B) anodes for lithium-ion batteries with high-power and long-life performance. The spherical TiO_2(B) electrodes with a small amount of a carbon conductor additive had a high electrode density of 2.2 g cm^{-3} and a volumetric reversible capacity of 475 mAh cm^{-3} comparable to that of graphite electrodes. Compared with nano-size needle-like TiO_2(B) electrodes, the spherical TiO_2(B) electrodes exhibited higher-rate discharge capability and longer-cycle life performance. The impedance of the TiO_2(B)/electrolyte interface model indicated that the charge transfer resistance R_c and the passivating film resistance R_f of the spherical TiO_2(B) were much smaller than those of the needle-like one. The high-rate discharge and the long-cycle performance of the spherical TiO_2(B) electrode are attributed to the superior electronic connective property and R_c and R_f values smaller than those of the needle-like one. Lithium-ion cells using the spherical TiO_2(B) anodes and $LiNi_{0.8}Co_{0.1}Mn_{0.1}O_2$ cathode with a capacity of 2.8 Ah exhibited a high energy density of 100 Wh kg^{-1}, a high output power density of 1800 W kg^{-1} for 10 s pulse, and a long cycle life of more than 3000 cycles.

1. Introduction

Development of large-scale lithium-ion batteries for automotive and stationary power storage applications has been progressing with a view to enhancing power, energy density, safety, life, quick-charge, and low-temperature performance. However, with regard to conventional lithium-ion batteries using graphite anodes for

* Corresponding author. Tel.: +81 44 549 2120; fax: +81 44 520 1286.
E-mail address: yasuhiro3.harada@toshiba.co.jp (Y. Harada).

http://dx.doi.org/10.1016/j.jpowsour.2014.09.170
0378-7753/

these applications, there are important issues concerning limitations on life, safety, and low-temperature performance. For example, quick-charging and charging at low temperature lead to detrimental effects, namely, short cycle life and a safety issue because of the lithium plating on the surface of graphite anodes in lithium-ion batteries. Therefore, 1.5 V anode materials such as spinel $Li_{4/3}Ti_{5/3}O_4$ (LTO) and titanium dioxides (TiO_2), for example, anatase, rutile, monoclinic (TiO_2(B)), and brookite [1], have been extensively studied as anode materials in view of their life and safety superior to those of graphite and considering that their use would render lithium metal plating unnecessary. In particular, LTO is expected to be an attractive electrode material with zero-strain property, nano-sized particle, thermal stability, safety properties [2–11]. It has been demonstrated that lithium-ion batteries using LTO as the anode material offer high-power, quick-charging, long-life, and safety [9–14] and such batteries have been developed for automotive and stationary power storage applications [11,13,14]. TiO_2 is also an attractive anode material because its theoretical capacity (335 mAh g^{-1}) is larger than that of LTO (175 mAh g^{-1}). However lithium insertion and extraction for anatase, brookite, and rutile TiO_2 is very slow, causing low rate capability and small reversible capacities in the case of use as a practical anode. Nano-seize TiO_2 powders have been studied in order to achieve high-rate performance.

Monoclinic TiO_2(B) materials with various nanostructures such as nanowire and nanotube have been synthesized and are also expected to be as attractive anode materials because TiO_2(B) exhibits higher reversible capacities and better cyclability than the other three forms of TiO_2. Lithium insertion into TiO_2(B) particles by electrochemical reaction has been reported by several researchers [15–19]. A relatively low reversible capacity of less than 200 mAh g^{-1} has been reported for TiO_2(B) synthesized by a solid–state reaction [15–17]. TiO_2(B) nanowire [20,21] and nanotube [22,23] prepared by hydrothermal reaction exhibited a high reversible capacity of 240–280 mAh g^{-1}. Compared with bulk forms, nanostructured forms of TiO_2(B) enhance the reversible capacity and the rate capability. TiO_2(B) nanoparticles prepared by hydrothermal reaction also indicated a high reversible capacity of 247 mAh g^{-1} and a significantly high rate capability [24]. However, a tap density of nanoparticulate TiO_2(B) is lower than that of the bulk, which results in a low volumetric energy density of the battery. The coulombic efficiency at the first cycle decreases with the particle size, which also results in the low energy density. It is necessary to use TiO_2(B) electrodes with a large amount of carbon conductor additive, such as ketjen black (KB) or acetylene black (AB), in order to enhance the electrode performance, but the additive causes low electrode density. Satio et al. reported that an optimized TiO_2(B) composite electrode with 10 wt% KB additive showed the highest gravimetric discharge capacity of 314.4 mAh g^{-1} but a low volumetric discharge capacity of 233 mAh cm^{-3} because of the low electrode density of 0.74 g cm^{-3} [25].

We have also studied synthesis conditions, electrochemical properties, and lithium storage of TiO_2(B) prepared by the solid–state reaction in order to understand the effects of the reversible capacity, cycle performance, and the rate capability of anode [26,27]. To further develop TiO_2(B) anode for practical lithium-ion batteries with high-density electrode, high-power, and long-life performance, it is necessary to improve the rate capability, coulombic efficiency, and cycle life performance of TiO_2(B) electrodes by using high-density TiO_2(B) electrodes. In our investigation of the promising TiO_2(B) particles for the anode application, we compared the electrochemical properties of micro-size spherical TiO_2(B) and nano-size TiO_2(B) particles. The micro-size spherical TiO_2(B) particles are expected to realize high-density electrodes because spherical particles have a high tap density. This paper reports on the electrochemical properties and performance of micro-size spherical TiO_2(B) secondary particles applied as anode materials in lithium-ion batteries for automotive and stationary power applications.

2. Experimental

The micro-size spherical TiO_2(B) particles were prepared by following method. The precursor $K_2Ti_4O_9$ was prepared by a conventional solid–state reaction method. The mixture of raw materials such as K_2CO_3 and TiO_2 was dispersed in distilled water with a concentration of 470 g L^{-1}. The mixed slurry was spray dried to form secondary particles with an average size of 15 μm at Titan Kogyo,Ltd., which was heated at 1000 °C for 1 h. The granulated $K_2Ti_4O_9$ particles were proton exchanged with 1.8 mol l^{-1} H_2SO_4 to obtain $H_2Ti_4O_9$ as an intermediate compound. Finally, micro-size spherical TiO_2(B) secondary particles were obtained by dehydrating the intermediate powder as reported in our previous paper [26]. To make comparison of primary and secondary particles of TiO_2(B) on electrochemical properties, the spherical TiO_2(B) secondary particles were disintegrated by grinding to obtain the needle-like TiO_2(B) primary particles.

Fig. 1 shows SEM images of the spherical TiO_2(B) secondary and the needle-like primary particles. The spherical secondary particle consists of nano-size needle-like TiO_2(B) primary particles. Average particle sizes (diameter) of the spherical TiO_2(B)

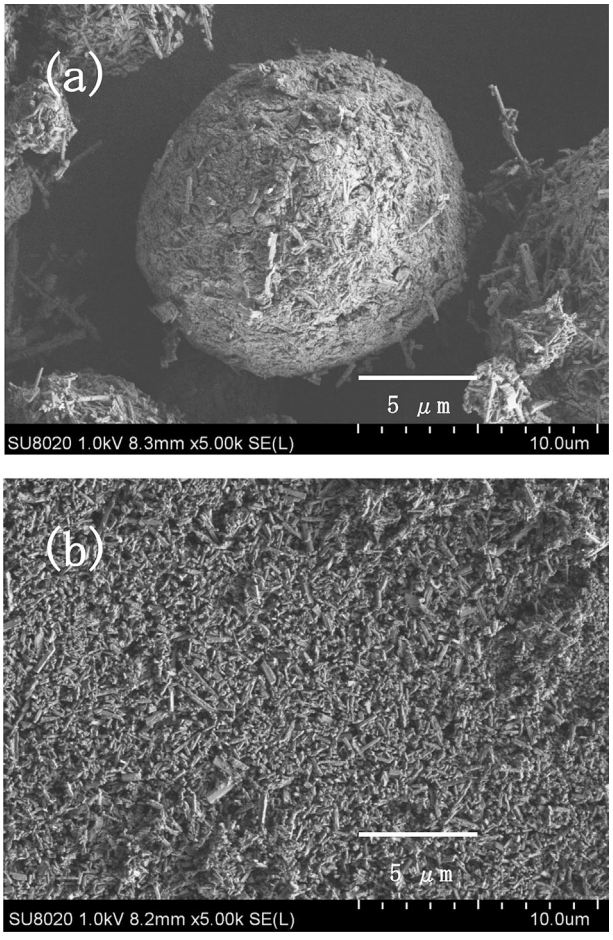

Fig. 1. SEM images of spherical TiO_2(B) secondary particles (a) and needle-like TiO_2(B) primary particles (b).

secondary particles and the needle-like primary particles were about 10 and 0.5 μm, respectively. Brunauer-Emmett-Teller (BET) specific surface areas of the spherical TiO_2(B) secondary particles and the needle-like primary particles were 17.7 and 19.2 $m^2\ g^{-1}$, respectively.

The TiO_2(B) composite electrodes were prepared from a paste mixture of 92 wt% TiO_2(B) powder, 2 wt% carboxymethylcelluose (CMC) binder, 2 wt% styrene-butadiene (SBR) binder, and 4 wt% AB conductor in an aqueous solution. The paste was coated on aluminum foil and then dried. The TiO_2(B) electrodes were pressed to obtain the electrode density of 2.2 g cm^{-3}. $Li_{4/3}Ti_{5/3}O_4$ (LTO) composite electrode was also prepared in the same manner as described previously [12] in order to compare the performance of TiO_2(B) electrodes. The average particle size of LTO was about 0.9 μm. The electrodes were dried under vacuum at 85 °C for 24 h before electrochemical measurements. Electrochemical measurements were performed by using the spherical TiO_2(B), the needle-like TiO_2(B), and the LTO electrodes with electrode material loading of 2 and 10 mg cm^{-2} on the aluminum foil corresponding to the electrode thicknesses of 9 and 45 μm.

Charge (lithium insertion)-discharge (lithium extraction) cycling tests, rate performance, and impedance measurements of the TiO_2(B) and the LTO electrodes were carried out using a three-electrode glass cell constructed using the TiO_2(B) or the LTO electrodes (2 × 2 cm), a Li metal chip reference electrode, a Li metal counter electrode, a glass filter separator, and a 1 M $LiPF_6$ in a mixed ethylene carbonate (EC) and diethyle carbonate (DEC) (1:2 by volume) electrolyte. Galvanostatic charge–discharge cycling tests of the TiO_2(B) electrodes were carried out between 1.3 and 3 V at 100 mA g^{-1}. 1 C rate for TiO_2(B) and LTO electrode are 200 and 170 mA g^{-1}, respectively. Impedance measurements of the TiO_2(B) electrodes were carried out under the open-circuit potentials between 1.1 and 1.59 V vs. Li/Li^+ after charging in the frequency range of 3 × 10^5 to 5 × 10^{-2} Hz. All experiments were carried out at 24–25 °C in a dry atmosphere. We determined the charge-transfer resistance R_c and the passivating film resistance R_f, using an equivalent circuit consists of two parallel circuits in series. We used a frequency range of 19 Hz–60 kHz for R_c and 0.3 Hz–190 Hz for R_f, respectively.

Prototype TiO_2(B)/$LiNi_{0.8}Co_{0.1}Mn_{0.1}O_2$ (NCM) pouch cells with a capacity of 2.8 A h were used in order to evaluate cycle life, discharge rate performance, and power capability for automotive and stationary power applications. The TiO_2(B)/NCM cells were constructed by using the spherical TiO_2(B) anode with the electrode material loading of 10 mg cm^{-2}, the NCM cathode with the electrode material loading of 9.2 mg cm^{-2}, an electrolyte, a polyethylene separator, and a laminated film pouch case. The NCM cathode was prepared from a paste mixture of 92.6 wt% NCM powder from a commercial sample, 2.8 wt% poly(vinylidene fluoride) binder, and 4 wt% carbon conductor in N-methyl pyrrolidone. The paste was coated on aluminum foil and then dried. The NCM cathode was pressed to obtain the electrode density of 3.2 g cm^{-3}. The anode–cathode capacity balance in cells was set to be almost equal. The electrolyte was a 1 M solution of $LiPF_6$ in a mixed propylene carbonate (PC) and DEC (1:2 by volume) solvent.

The discharge performance of TiO_2(B)/NCM cell was measured at 25 °C by various discharge currents from 0.56 to 22.4 A down to 1.5 V after CC-V (constant current-constant voltage) charging at 2.8 A constant current up to 2.9 V of constant voltage to 0.14 A of cut-off current. We selected 1 C rate of 2.8 A. Charge-discharge cycling tests were carried out between 2.9 V and 1.5 V at 1 C rate at 25 °C. The power densities for output and input for 10 s were calculated from Hybrid Pulse Power Characterization (HPPC) test [28].

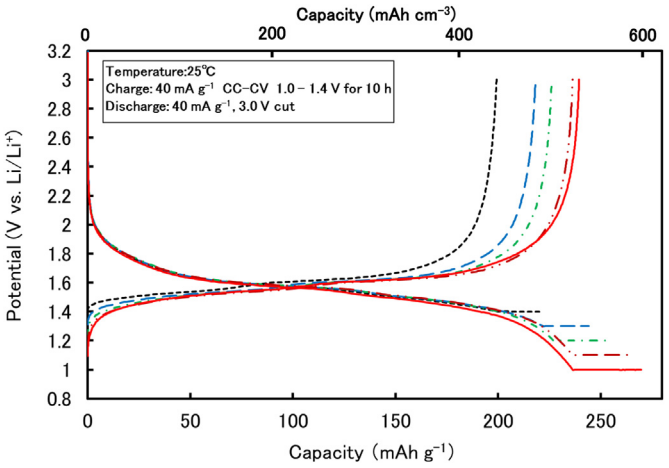

Fig. 2. Charge–discharge potential curves of the spherical TiO_2(B) electrodes with different minimum charge potentials between 1.0 and 1.4 V at the first cycle.

3. Results and discussion

3.1. Electrochemical properties of TiO_2(B) electrodes

Electrochemical properties of lithium insertion and extraction for TiO_2(B) have been characterized by galvanostatic charge (lithium insertion) - discharge (lithium extraction) tests. Fig. 2 shows the charge–discharge potential curves of the spherical TiO_2(B) electrodes at various charge cut-off potentials at the first cycle. The discharge capacity (reversible capacity) increased with decreasing the charge cut-off potential from 1.4 to 1.0 V vs. Li/Li^+. Gravimetric reversible capacity and volumetric reversible capacity after 1.0 V charging were 240 mAh g^{-1} and 528 mAh cm^{-3}, respectively. However, lithium insertion into TiO_2(B) at the lower potential below 1.3 V vs. Li/Li^+ had a large polarization [27], which means that in the practice the TiO_2(B) anode takes a long time to become fully charged below 1.3 V. The low potential limit for TiO_2(B) should be set at 1.2 V vs. Li/Li^+ or higher because of the improvement for cyclability [29]. Therefore, charge–discharge cycling tests of TiO_2(B) electrodes were performed between 1.3 and 3 V. Fig. 3 shows a comparison of charge–discharge

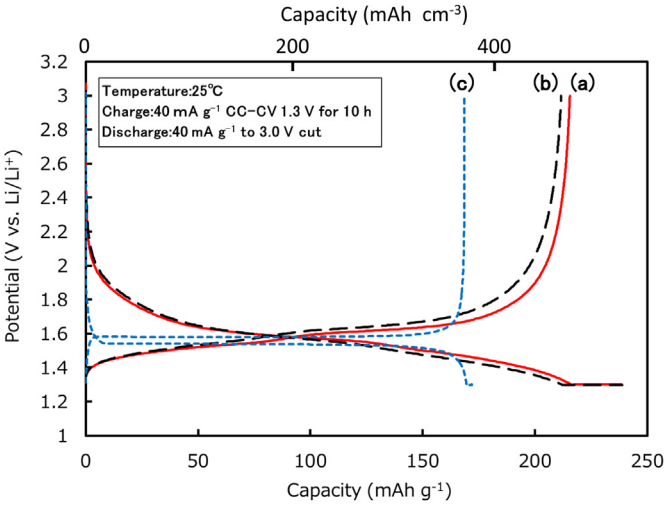

Fig. 3. Comparison of charge–discharge potential curves of the spherical TiO_2(B) (a), the needle-like TiO_2(B) (b), and LTO (c) electrode between 1.3 and 3.0 V vs. Li/Li^+ at the first cycle.

properties of the spherical TiO_2(B), the needle-like TiO_2(B), and the LTO electrode at the first cycle. The spherical and the needle-like TiO_2(B) electrode had high gravimetric reversible capacities of 216 mA g^{-1} and 212 mA g^{-1}, respectively compared to that of LTO electrode (169 mAh g^{-1}). The volumetric reversible capacity of the spherical TiO_2(B) electrodes was 475 mAh cm^{-3}, which is comparable to that of graphite electrodes with the electrode density of ca. 1.4 g cm^{-3} [30,31]. The coulombic efficiency of the spherical TiO_2(B), the needle-like TiO_2(B), and the LTO electrodes at the first cycle was 90.4, 88.7, and 98%, respectively. These values of TiO_2(B) electrodes were lower than that of the LTO electrode. Therefore, it is necessary to select a high-capacity cathode material with the coulombic efficiency of around 90% if the higher capacity of TiO_2(B) than that of LTO is available for practical battery use. $LiNi_xCo_yMn_{1-x-y}O_2$ (NCM) as the cathode in combination with TiO_2(B) anode is more promising than $LiCoO_2$ and $LiMn_2O_4$ because of the higher capacity and the lower coulombic efficiency for $LiNi_xCo_yMn_{1-x-y}O_2$ (NCM). The needle-like TiO_2(B) electrode had a larger polarization and a slightly lower coulombic efficiency than those of the spherical TiO_2(B) electrode. We consider that a small amount of carbon conductor additive in the needle-like TiO_2(B) electrode is insufficient to work as the electronic conductor. Therefore, influence of TiO_2(B) electrode thickness on the electrode performance has been investigated by the discharge-rare performance tests of the TiO_2 (B) electrodes with two different thicknesses.

Fig. 4 shows discharge potential curves of the spherical and the needle-like TiO_2(B) thin electrode with the loading of 2 mg cm^{-2} at various discharge rates of 0.2–20 C. The spherical TiO_2(B) thin electrode had the higher capacities with a smaller polarization at more than 10 C rate (2000 mA g^{-1}) than those of the needle-like one. The discharge capacities of spherical and needle-like TiO_2(B) thin electrodes at a high rate of 20 C (4000 mA g^{-1}) were 176 and 113 mAh g^{-1}, respectively. The capacity retention of spherical and needle-like TiO_2(B) thin electrode at 20 C rate were 83 and 54%, respectively. Fig. 5 shows the discharge potential curves of the spherical and the needle-like TiO_2(B) thick electrodes with the loading of 10 mg cm^{-2} at various discharge rates of 0.2–10 C. It was clearly observed that the needle-like TiO_2(B) thick electrode had a large capacity fading with a large polarization at more than 1 C rate whereas the spherical TiO_2(B) thick electrode did not. Fig. 6 shows discharge rate capability of thin and thick electrodes with the spherical, the needle-like TiO_2(B), and the LTO. The rate capability of the spherical TiO_2(B) thin electrode was superior to that of the needle-like one and comparable to that of LTO thin

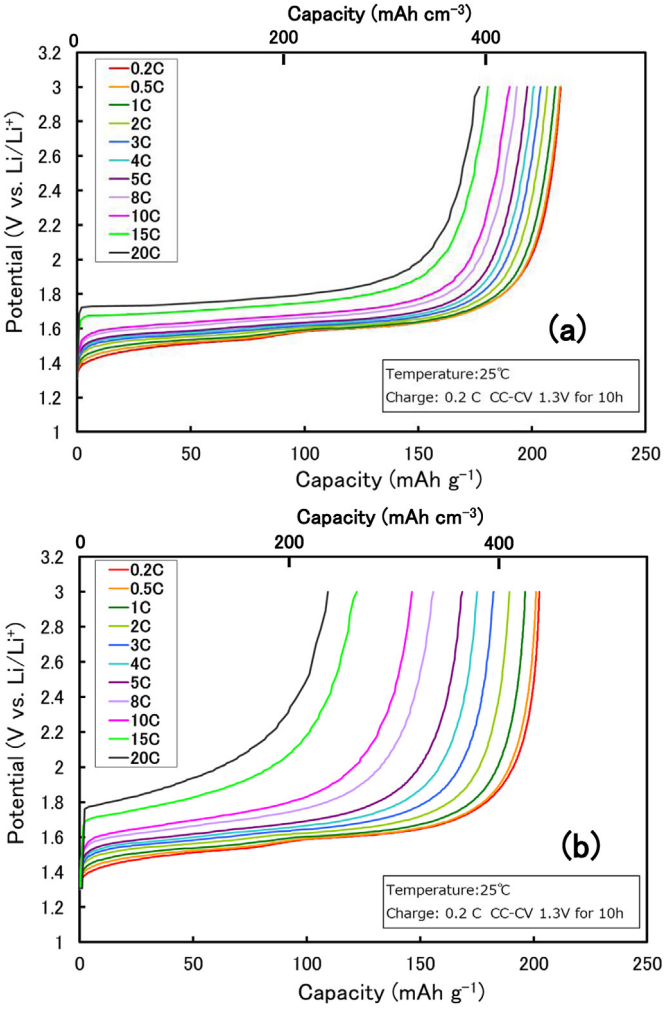

Fig. 4. Discharge potential curves of the spherical TiO_2(B) (a) and the needle-like TiO_2(B) (b) thin electrode with 9 μm thickness at various discharge rates. 1 C rate: 200 mA g^{-1}.

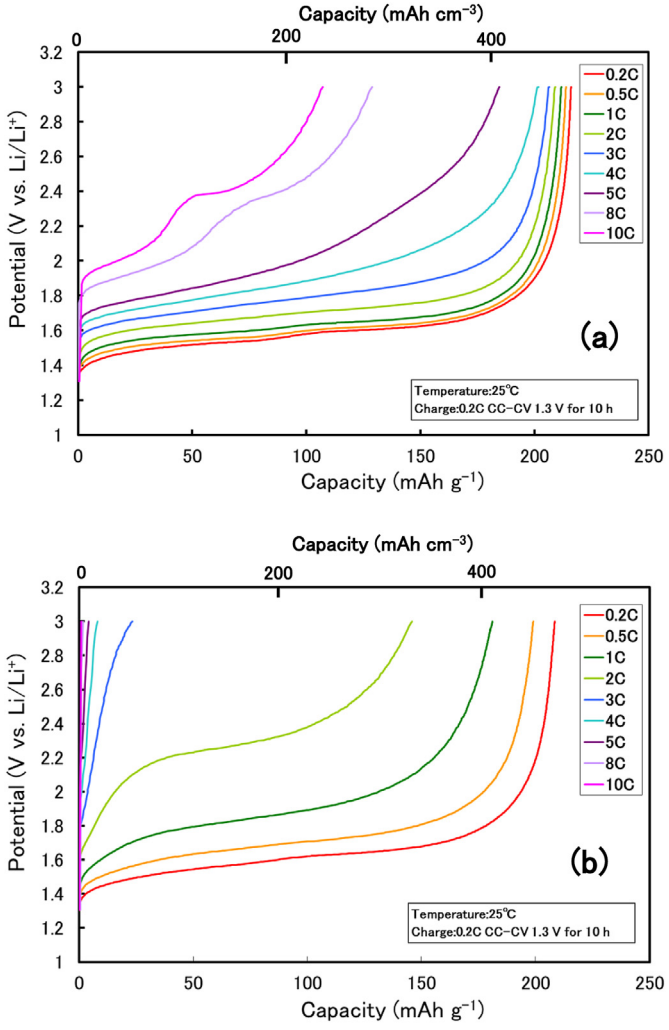

Fig. 5. Discharge potential curves of the spherical TiO_2(B) (a) and the needle-like TiO_2(B) (b) thick electrode with 45 μm thickness at various discharge rates. 1 C rate: 200 mA g^{-1}.

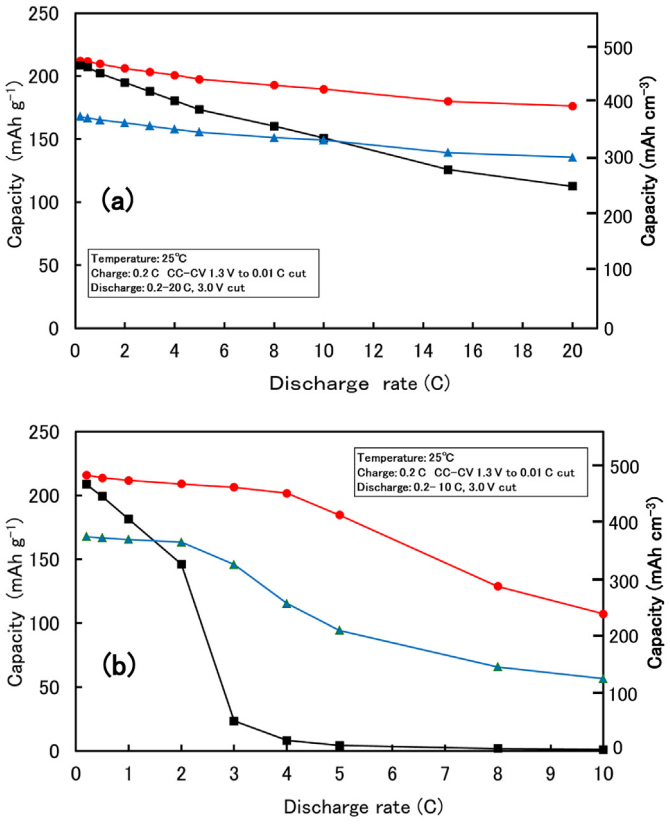

Fig. 6. Discharge capacities of the thin electrodes (a) and the thick electrodes (b) of the spherical TiO_2(B) (-●-), the needle-like TiO_2(B) (-■-), and the LTO (-▲-) at various discharge rates. 1 C rate for TiO_2(B) and LTO electrode are 200 mA g^{-1} and 170 mA g^{-1},respectively.

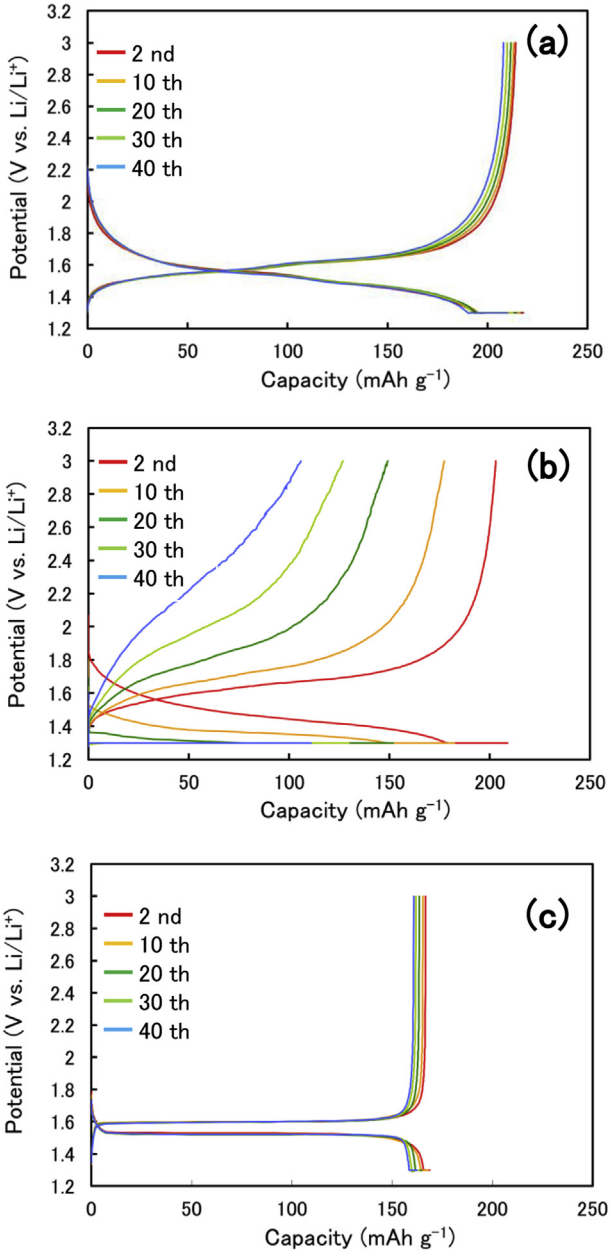

Fig. 7. Variations in the charge–discharge potential curves of the spherical TiO_2(B) (a), the needle-like TiO_2(B) (b), and LTO (c) thick electrode during the cycles at 0.5 C rate.

electrode. In the case of thick electrodes, it was noted that the discharge rate capability of the spherical TiO_2(B) thick electrode was considerably superior to that of the needle-like TiO_2(B) and the LTO electrodes. We consider that the electronic connection between the micro-size spherical TiO_2(B) secondary particles and a small amount of the carbon conductor additive is much better than that of the needle-like TiO_2(B) and the fine LTO particles, which maintains good homogeneous electrochemical reaction in the thick electrode even at high rate discharge. Therefore, the spherical TiO_2(B) secondary particles are suitable for used as the thick anodes in lithium-ion batteries to enhance the energy density. Figs. 7 and 8 show cycle performance of the spherical TiO_2(B), the needle-like TiO_2(B), and the LTO thick electrode. The spherical TiO_2(B) and the LTO electrodes exhibited a small change in the voltage curves during the cycles. The needle-like TiO_2(B) had a large polarization and a large capacity fading during the cycles. The cyclability of the spherical TiO_2(B) thick electrode was considerably superior to that of the needle-like one and comparable to that of the LTO thick electrode. The spherical TiO_2(B) and the LTO electrodes had a very small increase in polarization as the cycle number proceeded. On the contrary, the capacity of the needle-like TiO_2(B) electrode decreased considerably with increasing the polarization. These results indicate that maintaining high electronic conductivity in TiO_2(B) electrodes during the charge–discharge cycling is very important for good cyclability. The spherical TiO_2(B) secondary particles have an advantage of a very good electronic connection between TiO_2(B) particles and the carbon conductor during cycling, which leads to good cyclability of the TiO_2(B) with the high electrode density.

3.2. Impedance spectroscopy of TiO_2(B) electrodes

Fig. 9 shows typical AC-impedance spectra of spherical and needle-like Li_xTiO_2(B) electrodes at $x = 0.63$ after the first charge–discharge cycle. The impedance spectrum exhibits a depressed semicircle or a few semicircles in the higher frequency range and a straight line in the lower frequency range. We consider that the semicircle can be interpreted as resulting from the charge-transfer process and the passivating film formed on the TiO_2(B). TiO_2(B) particles with a large surface area are the electrochemically active and react with the electrolyte below 1.5 V vs. Li/Li^+, which leads to formation of the passivating product on a fresh TiO_2(B) surface. The semicircle of the needle-like TiO_2(B) electrode was larger than that of the spherical TiO_2(B) electrode. The impedance of the TiO_2(B)/electrolyte interface was modeled by a simple equivalent circuit as shown in Fig. 9. The equivalent circuit consists of two parallel

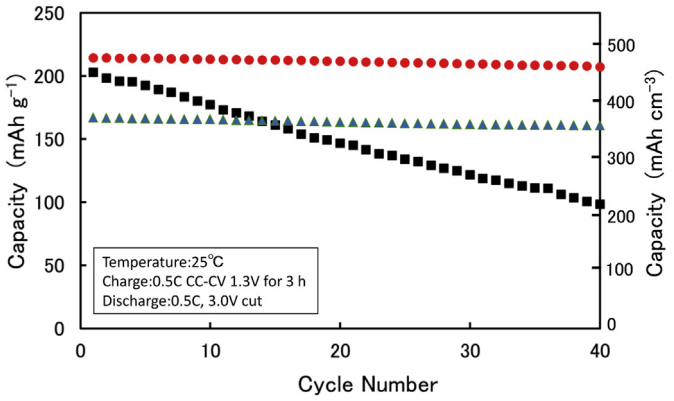

Fig. 8. Discharge capacities vs cycle number of the spherical TiO_2(B) (●), the needle-like TiO_2(B) (■), and the LTO (▲) thick electrode.

circuits in series. R_o is the ohmic resistance, and R_c and R_f are the charge-transfer resistance and the passivating film resistance, respectively. W is the Warburg impedance, and C_d and C_f are capacities corresponding to R_c and R_f, respectively. Variation of the impedance spectra of TiO_2(B) electrodes with lithium insertion was characterized by using the equivalent circuit. Fig. 10 shows variation of R_c and R_f with x in Li_xTiO_2(B). R_c varied significantly with x. Such a variation of R_c for TiO_2(B) electrodes is caused by the charge-transfer resistance for lithium insertion into TiO_2(B) with a single-phase reaction. It is noted that R_c for the spherical TiO_2(B) is much smaller than that of the needle-like one. Specifically, the difference of R_c between spherical and needle-like TiO_2(B) increased with a decrease in x of <0.6. The electronic conductivity of TiO_2(B) is gradually changed from a conductor to an insulator with decreasing x value. This phenomena would result in a small available surface area for the charge transfer reaction in the range of $x < 0.6$, especially in the needle-like TiO_2(B) electrode due to its poor electronic condition path. We consider that the electronic connection between the spherical TiO_2(B) particles and the carbon conductor is much better than that of the needle-like one.

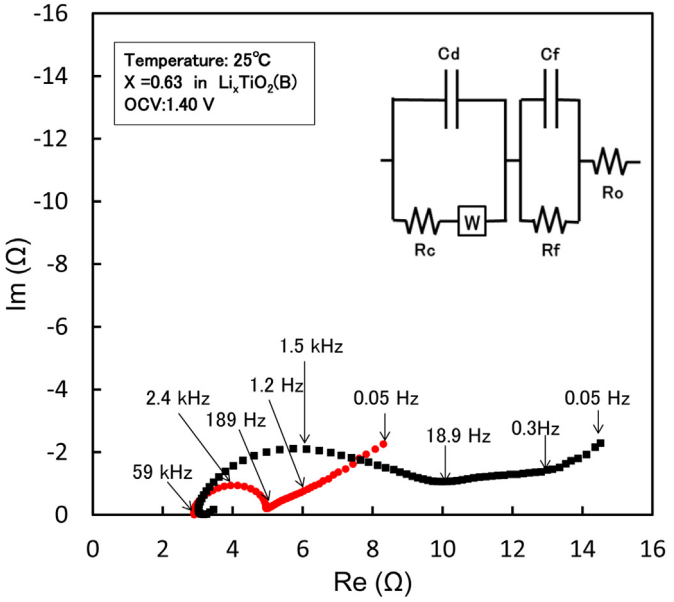

Fig. 9. AC-impedance spectra of the spherical TiO_2(B) (●) and the needle-like TiO_2(B) (■) thick electrode at 1.4 V.

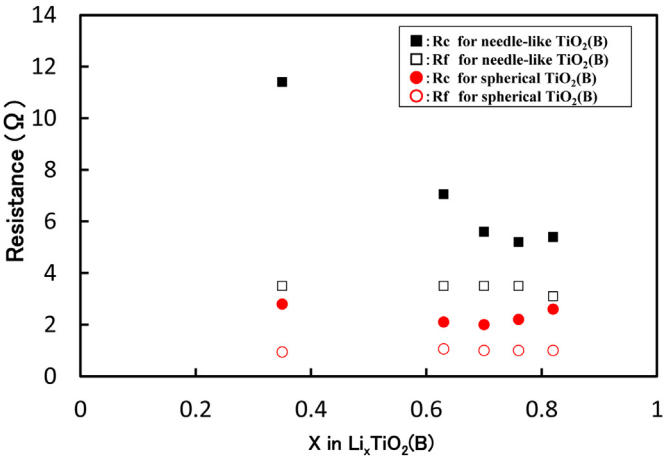

Fig. 10. Variations of R_c and R_f for the spherical TiO_2(B) and the needle-like TiO_2(B) electrode with x in Li_xTiO_2(B).

Therefore, by using TiO_2(B) electrodes containing even a small amount of carbon conductor additive, the spherical TiO_2(B) particles with the good electronic connective property are considered to have a large available surface area for the charge transfer reaction of lithium insertion and extraction. R_f was independent of x because R_f is associated with the film. R_f for the needle-like TiO_2(B) electrode was larger than that for the spherical TiO_2(B) electrode. We consider that such a larger R_f for the needle-like TiO_2(B) electrode is due to the thicker film formation. The high-rate discharge and the long-cycle life performance of the spherical TiO_2(B) electrode are attributed to the R_c and R_f values smaller than those of the needle-like one.

3.3. Performance of prototype TiO_2(B)/NCM cells

Prototype TiO_2(B)/NCM pouch cells with a combination of the spherical TiO_2(B) thick anode and a $LiNi_{0.8}Co_{0.1}Mn_{0.1}O_2$ cathode have been developed for enhancing the energy density because the $LiNi_{0.8}Co_{0.1}Mn_{0.1}O_2$ cathode had a high capacity of 175 mAh g^{-1} and a coulomic efficiency of 89% that was almost the same as that of the TiO_2(B) anode at the first cycle. The specifications of the TiO_2(B)/NCM cell are summarized in Table 1. The nominal capacity, the nominal voltage, and the energy density were 2.8 Ah, 2.3 V, and 100 Wh kg^{-1}, respectively. Discharge curves of the TiO_2(B)/NCM cell at various discharge rates are shown in Fig. 11. The discharge capacity curves at 4 C (11.2 A) and 8 C (22.4 A) rate showed the capacity retention of 88.5 and 55.5%, respectively. The discharge rate capability decreased considerably at more than 4 C rate. Such a rate capability is acceptable for stationary power applications but insufficient for plug-ion hybrid electric vehicle (PHEV) and electric vehicle (EV) applications. Fig. 12 shows pulse-power capability for

Table 1
Specifications of prototype TiO_2(B)/$LiNi_{0.8}Co_{0.1}Mn_{0.1}O_2$ cell.

Cell	TiO_2(B)/NCM cell
Case	Al laminated film
Dimension (mm)	110 × 72 × 4.3
Weight (g)	64
Nominal capacity (Ah)	2.8
Nominal voltage (V)	2.3
10 s output power density (W kg^{-1})[a]	1800
10 s input power density (W kg^{-1})[a]	2600
Energy density (Wh kg^{-1})	100

[a] At 50%SOC and 25 °C.

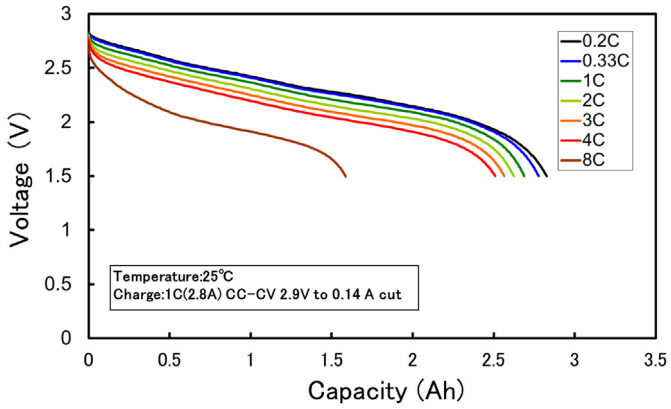

Fig. 11. Discharge curves of the TiO_2(B)/$LiNi_{0.8}Co_{0.1}Mn_{0.1}O_2$ cell at various discharge rates. 1 C rate: 2.8 A.

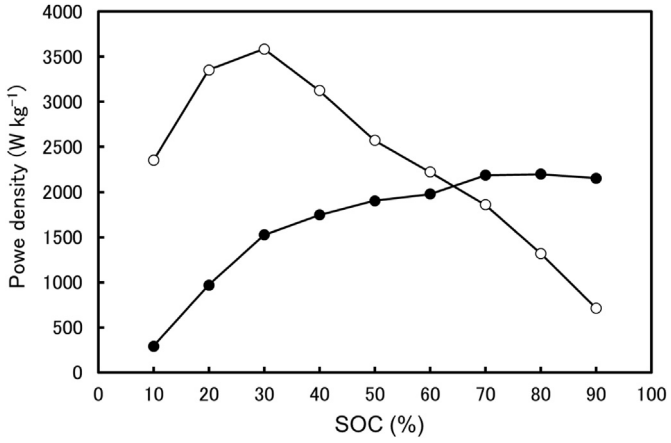

Fig. 12. Input and output power capability of the TiO_2(B)/$LiNi_{0.8}Co_{0.1}Mn_{0.1}O_2$ cell at 25 °C for 10 s pulse by HPPC testing.

the TiO_2(B)/NCM cell obtained by HPPC testing at 25 °C. The maximum output and input power density for 10 s at 50%SOC were 1900 W kg^{-1} and 2500 W kg^{-1}. The input power density of more than 2500 W kg^{-1} was maintained in the low SOC range of 20–50 %, which is suitable for regenerating in plug-in hybrid electric vehicles (PHEV). The output power density of more than 1500 W kg^{-1} was maintained at more than 30% SOC. The discharge rate and the output power were inferior to those of LTO/NCM cell [14]. Further improvement of both the discharge rate performance and the output pulse-power capability is necessary for PHEV and EV applications.

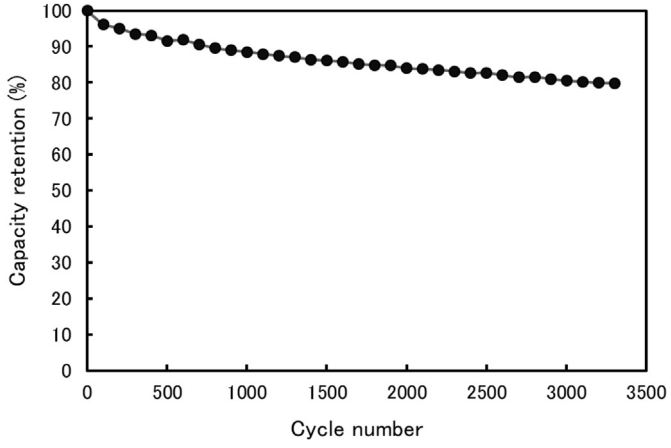

Fig. 13. Cycle performance of the TiO_2(B)/$LiNi_{0.8}Co_{0.1}Mn_{0.1}O_2$ cell at 25 °C and 1 C rate.

Fig. 13 shows cycle life performance of the TiO_2(B)/NCM cell by the charge–discharge cycling at 1 C rate between 1.5 and 2.9 V in 100% SOC width. The capacity retention after 3000 cycles was 80%, which is acceptable for EV and stationary power applications. However, the cycle life performance of the TiO_2(B)/NCM cell should be further improved to be comparable to that of the LTO/NCM cell [14]. We consider that the capacity decline during the cycling is mainly caused by an increase in resistance for TiO_2(B) anodes because TiO_2(B) has a large surface area and a larger volume change during the cycling compared to that of LTO. Therefore, we are now developing TiO_2(B) with the long cycle performance comparable to LTO.

4. Conclusions

In our investigation of the electrochemical properties and the performance of micro-size spherical TiO_2(B) secondary particle anodes for high-power and long-life lithium-ion batteries, we compared those of needle-like TiO_2(B) and LTO particles. The spherical TiO_2(B) electrodes with the high electrode density of 2.2 g cm^{-3} to which a small amount (4 wt%) of AB conductor was added had a high coulombic efficiency of 90% at the first cycle and a reversible volumetric reversible capacity of 475 mAh cm^{-3} (216 mAh g^{-1}) after 1.3 V vs. Li/Li^+ charging, which values are comparable to those of graphite. Comparison of discharge rate capability and cycle life performance of the spherical TiO_2(B), the needle-like TiO_2(B), and the LTO electrodes revealed that the discharge rate and the cycle life performance of the spherical TiO_2(B) electrodes were considerably superior to those of the needle-like TiO_2(B) electrodes. The decline in the discharge rate capability of the spherical TiO_2(B) thick electrode was smaller than that of the needle-like TiO_2(B) thick electrode. Impedance spectrum of the spherical TiO_2(B) electrode was observed to be significantly smaller than that of the needle-like one. The impedance of TiO_2(B)/electrolyte interface model indicated that the charge transfer resistance R_c and the passivating film resistance R_f of the spherical TiO_2(B) were much smaller than those of the needle-like one. The spherical TiO_2(B) particles with a very good electronic connection between TiO_2(B) particles and the carbon conductor are considered to have a large available surface area for the charge transfer reaction. The high-rate discharge and the long-cycle life performance of the spherical TiO_2(B) electrode are attributed to the good electronic connective property and small values of R_c and R_f compared to those of the needle-like one. Lithium-ion cells using the spherical TiO_2(B) anodes and $LiNi_{0.8}Co_{0.1}Mn_{0.1}O_2$ cathodes have been developed for automotive and stationary power applications. It was demonstrated that the TiO_2(B)/$LiNi_{0.8}Co_{0.1}Mn_{0.1}O_2$ cells with a capacity of 2.8 Ah and a high energy density of 100 Wh kg^{-1} exhibited a high output power density of 1800 W kg^{-1} for 10 s pulse and a long cycle life of more than 3000 cycles.

References

[1] Z. Yang, D. Choi, S. Kerisit, K.M. Rosso, D. Wang, J. Zhang, G. Graff, J. Liu, J. Power Sources 192 (2009) 588.
[2] K.M. Colbow, J.R. Dahn, R.R. Haering, J. Power Sources 26 (1989) 397.
[3] N. Koshiba, K. Takata, M. Nakanishi, E. Asaka, Z. Takehara, Denki Kagaku 62 (1994) 870.
[4] E. Ferg, R.J. Gummow, A. de Kock, M.M. Thackeray, J. Electrochem. Soc. 141 (1994) L147.
[5] T. Ohzuku, A. Ueda, N. Yamamoto, J. Electrochem. Soc. 142 (1995) 1431.

[6] K. Nakahara, R. Nakajima, T. Matsushima, H. Majima, J. Power Sources 117 (2003) 131.
[7] L. Kavan, J. Prochzka, T.M. Spitler, M. Kalbac, M. Zukalova, T. Drezen, M. Gratzel, J. Electrochem. Soc. 150 (2003) A1000.
[8] A. Guerfi, S. Sevigny, M. Lagce, P. Hovington, K. Kinoshita, K. Zaghib, J. Power Sources 119-120 (2003) 88.
[9] M. Majima, S. Ujiie, E. Yagasaki, K. Koyama, S. Inazawa, J. Power Sources 101 (2001) 53.
[10] I. Belharouak, Y.K. Sun, K. Amine, J. Electrochem. Soc. 154 (2007) A1083.
[11] N. Takami, H. Inagaki, T. Kishi, Y. Harada, Y. Fujita, K. Hoshina, J. Electrochem. Soc. 156 (2009) A128.
[12] N. Takami, K. Hoshina, H. Inagaki, J. Electrochem. Soc. 158 (2011) A725.
[13] N. Takami, S. Kosugi, K. Honda, Toshiba Rev. 63 (12) (2008) 54.
[14] N. Takami, H. Inagaki, Y. Tatebayashi, H. Saruwatari, K. Honda, S. Egusa, J. Power Sources 244 (2013) 469.
[15] B. Zachau-Christiansen, K. West, T. Jacobsen, S. Atlung, Solid State Ionics 28-30 (1988) 1176.
[16] H. Kawamura, Y. Muranishi, T. Miura, K. Kishi, Denki Kagaku 59 (1991) 766.
[17] L. Brohan, R. Marchand, Solid State Ionics 9-10 (1983) 419.
[18] M. Zukalová, M. Kalbáč, L. Kavan, I. Exnar, M. Graetzel, Chem. Mater. 17 (2005) 1248.
[19] M. Inaba, Y. Oba, F. Niina, Y. Murota, Y. Ogino, A. Tasaka, K. Hirota, J. Power Sources 189 (2009) 580.
[20] A.R. Armstrong, G. Armstrong, J. Canales, P.G. Bruce, Angew. Chem. Int. Ed. 43 (2004) 2286.
[21] G. Armstrong, C. Arrouvel, V. Gentili, S.C. Parker, M.S. Islam, P.G. Bruce, Chem. Mater. 22 (2010) 6426.
[22] G. Armstrong, A.R. Armstrong, J. Canales, P.G. Bruce, Chem. Commun. (2005) 2454.
[23] G. Armstrong, A.R. Armstrong, J. Canales, P.G. Bruce, Electrochem. Solid State Lett. 9 (2006) A139.
[24] Y. Ren, Z. Liu, F. Pourpoint, A.R. Armstrong, C.P. Grey, P.G. Bruce, Angew. Chem. Int. Ed. 51 (2012) 2164.
[25] M. Saito, Y. Murota, M. Takagi, M. Tajima, T. Asao, H. Inoue, A. Tasaka, M. Inaba, J. Electrochem. Soc. 159 (2012) A49.
[26] Y. Harada, K. Hoshina, H. Inagaki, N. Takami, Electrochim. Acta 112 (2013) 310–317.
[27] K. Hoshina, Y. Harada, H. Inagaki, N. Takami, J. Electrochem. Soc. 161 (2014) A348–A354.
[28] Freedom CAR Battery Test Manual for Power Assist Hybrid Electric Vehicles DOE/ID-11069, Oct. 2003.
[29] Y. Murota, Y. Oba, M. Takagi, T. Asao, M. Saito, A. Tasaka, M. Inaba, Elecrochemisry 78 (2010) 431.
[30] N. Takami, A. Satoh, M. Hara, T. Ohsaki, J. Electrochem. Soc. 142 (1995) 2564.
[31] J. Shim, K.A. Striebel, J. Power Sources 119-121 (2003) 934.